Journal of Marine Research, 67, 569–595, 2009

Measuring turbulent large-eddy structures with an ADCP. Part 2. Horizontal velocity variance

by A. E. Gargett[1,2], A. E. Tejada-Martínez[3] and C. E. Grosch[1]

ABSTRACT

This paper considers the degree of accuracy with which observations from an acoustic Doppler current profiler (ADCP) can determine turbulent horizontal velocity variance. As in a previous paper addressing turbulent vertical velocity variance, we use a combination of techniques, deriving response functions from simple theory and from oceanic observations taken with a VADCP (an ADCP with an additional vertical (V) beam) in two different oceanic turbulent flows, Langmuir supercells (LSC) and unstable convection. In the case of LSC, we also determine response by sampling available Large-Eddy Simulations (LES) with specified beam geometry. In contrast with the previous investigation, where a direct measurement of vertical velocity variance was available from the vertical beam of the VADCP, we lack direct measurements of horizontal velocity variances. Thus the observational response reported here for horizontal variance is an estimate, taken as the ratio of first-order to the (assumed more accurate) second-order variance estimates made possible for the first time by the presence of a vertical beam.

The theoretical response function is used to illustrate effects on response of horizontal scale, vertical/horizontal anisotropy and possible quasi-coherent phase structure of the large eddies of the turbulent field, and to predict the impact of changing θ, the angle of slant beams from vertical. Observational estimates show that convective turbulence is characterized by near-unity response throughout the water column for both horizontal velocity variances, in agreement with theoretical prediction. For Langmuir supercells, theoretical responses correctly predict qualitative behavior of the LES-derived response functions, specifically overestimation in the lower part of the water column shifting to underestimation toward the surface. LES-derived responses for different values of θ are also in agreement with theory: both approaches suggest that $\theta = 30°$ provides more accurate measurement of horizontal turbulent velocity variance than does $\theta = 20°$, the present commercial standard.

For all examined cases of unstable convection and most (normal) LSC cases, observationally estimated response functions generally agree with theoretical (and, where available, LES) predictions. However in a few (abnormal) LSC cases, record-averaged second-order variances are clearly underestimated (most obviously when they are actually negative). We have been unable to assign a cause to this underestimation and advise against use of second-order horizontal velocity variances until this unpredictable effect is understood. Normal LSC cases exhibit overestimation of horizontal variance by a maximum factor of 1.5 (observational estimates) to 3 (LES estimates), a degree of

1. Center for Coastal Physical Oceanography, Old Dominion University, Norfolk, Virginia, 23508, U.S.A.
2. Institute of Ocean Sciences, Sidney, B.C., V8L 4B2, Canada. ***email: gargettann@gmail.com***
3. Department of Civil and Environmental Engineering, University of South Florida, Tampa, Florida, 33620, U.S.A.

accuracy comparable to that associated with microscale-based estimates of turbulent large-eddy quantities. We suggest ways in which the parameters needed for theoretical prediction of the response function for horizontal velocity can be estimated directly from VADCP measurements.

1. Introduction

A previous paper (Gargett *et al.,* 2008, henceforth Part 1) provided motivation for the use of Acoustic Doppler Current Profilers (ADCPs) for measurement of the large eddy scales of turbulence in the ocean. Briefly, the structure and variability of the energy-containing scales of turbulence contain direct links to the instability mechanism(s) that deliver energy to them, hence to a basic understanding of processes that generate ocean turbulence. Because of the well known three-dimensional turbulent cascades of kinetic energy and scalar variance, the dissipation scales that are usually defined as turbulence measurements actually contain no direct information about the processes that generated them, nor the vertical fluxes associated with them, fluxes essential for global ocean circulation and embedded ecosystems. Microscale profilers cannot measure the energy-containing scales of ocean turbulence, partly because some sensors, like airfoil probes, are band-limited by nature, but also because both freefall and self-propelled vehicles respond to motions of scales similar to their own dimensions, acting as an effective high-pass filter. Instead, energy-containing scales and turbulent fluxes have been inferred indirectly from measured microscale quantities using multiple assumptions, some of which are unproven or even doubtful. Even dissipation-scale isotropy is unlikely for many low Reynolds number patches (Gargett *et al.,* 1984), leaving the basic dissipation estimates uncertain within perhaps a factor of 2. In addition, constant mixing efficiency and a single eddy diffusivity for all scalars are suspect in the case of vertical fluxes, while the gradient-diffusion and turbulent viscosity relationships are themselves only hypotheses. It is thus highly desirable to measure the energy-containing and flux-carrying scales of ocean turbulence directly.

In shallow coastal waters, progress has been made toward this goal through bottom-mounted deployments of three types, bottom tripods heavily instrumented with point sensors (e.g. Sherwood *et al.,* 2006), bipolar acoustic systems (Stanton, 2001), and ADCPs. Major disadvantages of tripod systems include inability to measure the entire water column where it exceeds frame height (typically 1–2 m), as well as mechanical fragility which precludes measurements during the highly energetic wind/wave conditions characteristic of storms. The impact of this latter problem is clearly illustrated by the discovery (Gargett *et al.,* 2004) that storm-driven Langmuir supercells (LSC), full-depth Langmuir circulations occurring intermittently during the weakly stratified part of the year (September through May), are the dominant sediment transport mechanism at the inner shelf location of the LEO15 cabled observatory off the coast of New Jersey (for a map of the area, see http://explore.noaa.gov/long-term-ecosystem-observatory-at-15-meters-depth-leo-15). A number of years of tripod-based sediment transport studies at the same location completely missed this process because tripods were deployed only in the summer, a time of relatively calm wind/wave conditions and generally high upwelling-induced water column stratification. The combination of low Langmuir forcing and restriction of surface-forced motions

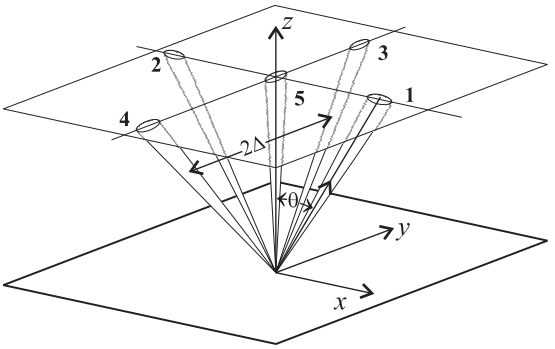

Figure 1. Bottom-mounted, upward-looking 5-beam VADCP. Slant beams make an angle of θ-30° from vertical. Horizontal separation of the slant beam pairs $2\Delta = 2z \tan\theta$ increases with distance z above the transducer. An instrument coordinate system is defined with vertical axis originating from the transducer face and horizontal axes defined in the orthogonal planes of the slant beam pairs, as shown.

to the part of the water column above the strong seasonal pycnocline results in the absence of LSC during the months suitable for tripod measurements. Bipolar acoustic systems produce highly desirable collinear velocity component profiles, but cannot be substantially scaled up in size to extend measurement beyond the near-bottom boundary layer (T. P. Stanton, pers. comm.), nor deployed on moorings or towed bodies. The use of ADCPs to measure turbulent quantities began in the 1990s, after development of pulse-to-pulse coherent and broadband sonar systems provided the accuracy needed to measure relatively small turbulent velocities in the sea. Over the past several years, both standard 4-beam ADCPs (Lohrmann *et al.,* 1990; Stacey *et al.,* 1999; Cheng *et al.,* 1999; Rippeth *et al.,* 2002; Lu and Lueck, 1999) and VADCPs, systems with an additional vertical beam (Gargett, 1994; Gargett and Wells, 2007, henceforth GW07), have been used to measure previously inaccessible characteristics of turbulence in shallow coastal locations. For ADCP-based measurements, the spatial arrangement of acoustic beams is a fundamental determinant of the ability to measure turbulence. Ideally, one would profile all three components of the instantaneous velocity vector along a vertical line, as bipolar systems do near bottom. Instead, a standard Janus-configuration ADCP measures radial velocities along pairs of opposing beams in 2 orthogonal planes, aligned respectively along x and y (instrument-based) axes (Fig. 1). Each beam in a pair makes an angle θ with the vertical z-axis,[4] defined with zero at the face of the transducer array. The centers of paired beams are separated by a distance $2\Delta(z) = 2z \tan\theta$ that increases with z. Under an assumption

4. Depending on the strength and frequency/wavenumber content of the flow field within which a turbulent field is embedded, significant instrument misalignment leads to irrevocable contamination of the turbulent field measurement. In this paper, it is assumed that the instrument has been accurately aligned to vertical, so fields calculated from combinations of slant beam velocities do not contain errors due to alignment, and the vertical fifth beam of a VADCP directly measures vertical velocity.

that the velocity field is uniform across the full beam spread (first-order homogeneity), estimates of horizontal velocity components are made from pairs of slant beams, while the standard estimate for vertical velocity uses all four beams. An assumption of uniformity over beam spread is reasonable for large-scale time-mean velocity fields but less comfortable for turbulence, which may contain a range of scales comparable to or smaller than the size of the 4-beam footprint at a particular height. It is thus of considerable interest to better understand the nature of the spatial response of an ADCP/VADCP for all six turbulent stresses (three normal stresses (variances), and three shear stresses) as functions of height and underlying turbulent structure. While this response will assuredly be less than ideal, it must be emphasized that there are presently **no** viable alternate methods for making measurements of the energy-containing eddies associated with the highly energetic but also highly intermittent turbulent events that dominate coastal waters during the several months every year when stratification is weak. Until such alternate methods arise, what knowledge we have of this large-scale turbulence in coastal waters will come from ADCPs.

In Part 1, we investigated the effect of the spatial configuration of a standard 4-beam ADCP on determination of turbulent vertical velocity variance. Methods used were a combination of simple theory, Large Eddy Simulation (LES), and field observations from the 2003 VADCP deployment that discovered Langmuir supercells (for deployment details, see GW07). Both theory and LES predict that the vertical velocity response function for turbulent velocities depends not only upon the horizontal spatial scale of the eddies relative to the maximum beam spread, but also upon the degree of vertical/horizontal anisotropy of the large eddies and the presence/absence of quasi-deterministic phase relationships among velocity components. Two different turbulent flows were selected from the observations, the LSC typical of storm conditions and unstable convection driven by surface heat loss at times of weak winds and waves: for details and examples of both flows, see Part 1. Convective eddies did not exhibit strong phase relationships; for observed vertical/horizontal anisotropy, near-uniform response with depth was both predicted and observed. In contrast, response functions for LSC are dominated by characteristically strong phase relationships among velocity components; predicted cross-wind response is near unity throughout the water column, while predicted downwind response is first an increasing underestimate with increasing distance from the transducer, becoming an overestimate in the upper part of the water column. These theoretical predictions agreed qualitatively, and to a large extent quantitatively, with responses determined from the LES of LSC and from the observations. For both turbulent flows, the worst estimator (that using all 4 slant beams) of vertical velocity variance was at most a factor of 2–3 different from the "true" value measured by the vertical beam: agreement could be further improved by choosing as the "true" estimate the larger of the two slant-beam estimates that are averaged to form the 4-beam estimate.

The present paper uses generally similar techniques to investigate how well turbulent horizontal velocity variances can be determined in the same turbulent flows employed and described in Part 1: a major difference is that we lack a "true" estimate of horizontal velocity

variance from the observations. Section 2 outlines the various estimates that can be made for horizontal variances. First-order estimates can be made with only an ADCP, while supposedly more accurate second-order estimates require information from the 5th beam of a VADCP. Characteristics of a theoretical response function for first-order variance are derived and examined in Section 3. LES techniques are reviewed briefly in Section 4, then used to determine the first-order response function for an instrument immersed in a wind- and wave-driven turbulent flow characterized by LSC. In Section 5, data from both LSC and unstable convective turbulence are used to determine observationally-based response functions estimated as the ratio of first- to second-order variances, a process that reveals a problem with second-order variances under certain conditions. Several possible sources of this problem are considered, but an acceptable explanation is not found. Section 6 compares observational response functions with theoretical predictions for convective turbulence and, in the case of LSC, with the LES-based responses.

2. Turbulent horizontal variance estimates with 4- and 5-beam Doppler profilers

Consider a three-dimensional velocity field $\underline{u}(x, y, z) = (u, v, w)$ in an instrument-based coordinate system (seen in Fig. 1) with origin at the transducer, z positive upwards, x positive in the direction from beam 2 toward beam 1, and y positive from beam 4 toward beam 3 (directed 90° to the right of beam 2). In this system, slant beam velocities (defined as positive if directed towards the transducer) at height z are given by

$$B_1 = -u(+\Delta(z), 0, z) \sin\theta - w(+\Delta(z), 0, z) \cos\theta \tag{1}$$

$$B_2 = u(-\Delta(z), 0, z) \sin\theta - w(-\Delta(z), 0, z) \cos\theta \tag{2}$$

$$B_3 = -v(0, +\Delta(z), z) \sin\theta - w(0, +\Delta(z), z) \cos\theta \tag{3}$$

$$B_4 = v(0, -\Delta(z), z) \sin\theta - w(0, -\Delta(z), z) \cos\theta \tag{4}$$

where $2\Delta(z) = 2z \tan\theta$ is the horizontal distance between opposing beams at height z. Vertical velocity can be directly measured by the vertical beam of a VADCP,

$$w(0, 0, z) = -B_5. \tag{5}$$

or estimated from the 4 beams of an ordinary ADCP by a form

$$w_{(1)} = -\frac{\sum_{i=1}^{4} B_i}{4 \cos\theta}, \tag{6}$$

that assumes *first-order homogeneity* (denoted by subscript (1)), i.e. that velocity structures have horizontal scale much larger than the distance between beams, so that $u(-\Delta, 0, z) = u(\Delta, 0, z)$, etc.

In statistically stationary turbulence, velocity $\underline{u} = \underline{U} + \underline{u}'$ is assumed to consist of two

parts, a mean field $\underline{U}(z) = (U(z), V(z), 0)$ that is a function only of z, and a three-dimensional fluctuating field $\underline{u}'$ with zero mean $<\underline{u}'> = 0$ and turbulent kinetic energy per unit mass $E = ½ <u'u' + v'v' + w'w'>$, where angle brackets denote a suitable averaging process.[5] In this case, the beam velocities $B_q = <B_q> + B_{qf}$, $q = 1, \ldots, 4$ are also made up of two parts, a mean $<B_q(z)>$ and a fluctuating part $B_{qf}(x, y, z)$ with zero mean $<B_{qf}> = 0$ and variance $<B_{qf}^2>$. With these assumptions, Eqs. (1)–(6) can be written for both mean and fluctuating components individually.

Under an assumption of first-order homogeneity as defined above, the fluctuating forms of Eqs. (1) and (2) can be solved for first-order estimates of fluctuating velocity, e.g.

$$u_1' = \frac{(B_{2f} - B_{1f})}{2 \sin \theta} \tag{7}$$

and associated horizontal velocity variance

$$< u'^2 >_{(1)} = \frac{< (B_{2f} - B_{1f})^2 >}{4 \sin^2 \theta}. \tag{8}$$

An equivalent expression for $<v'^2>_{(1)}$ involves velocities from beams 3 and 4.

Although the assumption of first-order homogeneity is acceptable for mean flows, defined as those with horizontal spatial scales much larger than the maximum beam spread, it can be suspect for the scales that characterize turbulence. An alternate assumption is that of Lohrmann *et al.* (1990), who suggested that only second-order statistics need be uniform across the beam spread. Applying this much weaker assumption, which we term *second-order homogeneity,* to averaged equations for fluctuating beam variances yields equation pairs that can be solved for the horizontal velocity variances, provided that a direct measurement of vertical velocity is available from a 5th beam. Using the 2/1 beam pair as an example, at height z

$$< B_{1f}^2 > = < u_+'^2 > \sin^2 \theta + < w_+'^2 > \cos^2 \theta + < u_+' w_+' > \sin 2\theta \tag{9}$$

$$< B_{2f}^2 > = < u_-'^2 > \sin^2 \theta + < w_-'^2 > \cos^2 \theta - < u_-' w_-' > \sin 2\theta, \tag{10}$$

where subscripts $(+, -)$ denote values of u', w' measured in beams 1 and 2 at horizontal positions $x_1 = +\Delta(z)$ and $x_2 = -\Delta(z)$ respectively. Under second-order homogeneity, $<u_+'^2> = <u_-'^2> = <u'^2>$ etc., thus Eqs. (9) and (10) can be solved for a second-order estimate (subscript (2)) of the horizontal turbulence variance

5. The fluctuating velocity structures that can be observed at LEO15 must have periods longer than surface wave periods (from which they are separated by low pass filtering), and shorter than the dominant semi-diurnal tidal period. Because stable statistics typically require averaging over periods greater than an hour (see GW07) and tidal velocities can vary over this period, a linear least squares fit, computed separately at each bin, is first removed from the beam velocity time series. The averaging operator $<>$ denotes a subsequent time average over a period of one record ($\sim$ 2 h: individual records are referenced as sss.nnn, where nnn is the number of the record within session sss).

$$< u'^2 >_{(2)} = \frac{< B_{1f}^2 > + < B_{2f}^2 >}{2 \sin^2 \theta} - < B_{5f}^2 > \cot^2 \theta, \tag{11}$$

with a similar expression for $< v'^2 >_{(2)}$ derived from the 4/3 beam pair.

A standard ADCP provides only first-order variances while a VADCP also allows second-order estimates. The purpose of this paper is to assess the accuracy with which horizontal turbulent velocity variances are determined by first-order estimates, a process that is more difficult for horizontal variances than it was for the vertical variance considered in Part 1 because of the lack of groundtruth. Since both available observational estimates involve (different) assumptions and are affected (differently) by instrumental noise and sampling error, neither can be considered as "true". Consequently we will rely more heavily on a combination of the features of a theoretical response function (derived in Section 3) and those of the response derived by sampling LES available for LSC (Section 4). Favorable comparison of responses predicted by theoretical and LES methods with the "true" observational response that is available for vertical variance when using a VADCP (Part 1) gives confidence in applying these methods to horizontal variances in the absence of a "true" observational estimate. Response characteristics derived via these two methods can then be compared with an estimated observational response defined by assuming that the second-order variance is "true" (Section 5).

3. Theoretical response for horizontal turbulent velocity variance

The first attempt to derive a response function characterizing the spatial filtering effect of beam spread on measurement of horizontal velocity was that of Theriault (1986), who derived a theoretical response for (total) horizontal velocity u as a function of θ, z and k, where k is the horizontal wavenumber in the plane containing the beam pair used to estimate u. Theriault assumed that vertical velocity w is either identically zero ($w \equiv 0$) or else constant (i.e., $w_+ \equiv w(+\Delta, 0, z) = w(-\Delta, 0, z) \equiv w_-$): then letting $u = u_o \exp ikx$, he derived a response function for the first-order horizontal velocity variance,

$$R_T \equiv \frac{uu^*}{u_o^2} = \cos^2 (kz \tan \theta) = \cos^2 (k\Delta), \tag{12}$$

where star denotes complex conjugation. $R_T \leq 1$ for all k and has an infinite number of zeros at $k\Delta = n\pi/2$. Since turbulence spectra are typically red in wavenumber, the limit of horizontal resolution is usually taken as the first zero, corresponding to a cutoff length scale $\Lambda_c(z) = 4z \tan \theta$ that increases with distance from the transducer.

The Theriault response function R_T is the basis of existing belief that horizontal velocity variance at fixed wavelength becomes progressively underestimated with increasing range. However Theriault's assumptions about vertical velocity are inappropriate for turbulent velocity fields, in which the turbulent vertical velocity w' is expected to contain energy at wavenumbers similar to those of the horizontal turbulent velocity u'. A more general approach (following Gargett, 1994, and used in Part 1) extends Theriault's theory to

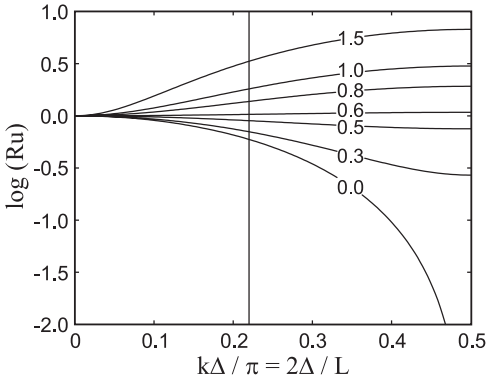

Figure 2. Logarithmic response functions for first-order horizontal velocity variance as functions of $k\Delta/\pi = 2\Delta/L$, where $2\Delta(z)$ is slant beam pair separation at height z above the transducer, and k and L are horizontal wavenumber and wavelength respectively. Curves are drawn for $\phi_o = 0°$ (zero phase lag between horizontal and vertical velocity components) and for the labeled values of vertical/horizontal anisotropy ratio w_o/u_o. The Theriault response function for non-turbulent flow is that with $w_o/u_o = 0$. For turbulent flows, response increases with w_o/u_o, switching from underestimation to overestimation at $w_o/u_o = 0.577$. The vertical line marks the location of a spatial scale of 80 m, typical of observed structures at LEO15, for a worst-case value of $\Delta(z) = \Delta_M = H \tan 30° = 8.66$ m, the maximum beam half-separation in water of mean depth $H = 15$ m.

"turbulent" velocities. Setting $u' = u_o \exp i(kx + ly)$ and $w' = w_o \exp i(kx + ly + \phi_o)$ allows for possible phase difference (ϕ_o) between u' and w' and for anisotropy in the sense of differences in their amplitudes, quantified by an anisotropy ratio w_o/u_o. The resulting response function for $<u'^2>_{(1)}$, the first-order estimate of horizontal velocity variance of a *turbulent* field is given by

$$Ru \equiv \frac{u'_{(1)}u'^*_{(1)}}{u_o^2} = \cos^2 k\Delta + r^2 \sin^2 k\Delta - r \sin \phi_o \sin 2k\Delta, \tag{13}$$

where $r = \dfrac{w_o}{u_o} \cot \theta$. The response for $<u'^2>_{(1)}$ is not affected by variation of the turbulent velocity field in the (y) direction normal to the plane of the beam pair used to calculate $u'_{(1)}$. However it does depend strongly on the $\{x, z\}$ structure of the underlying turbulent velocity fields through the anisotropy ratio w_o/u_o and the phase lag ϕ_o between u and w components.[6] Figure 2 illustrates the dependence of Ru on w_o/u_o for fixed $\phi_o = 0°$. The lowest curve ($w_o/u_o = 0$) is the Theriault response R_T (Eq.12), which is always an underestimate. For a turbulent velocity field, the response changes to *over*estimation for values of $w_o/u_o > 0.577$. Thus as a structure with fixed horizontal wavelength (say the ~

6. Taking $u = u_o \sin kx$, and $w = w_o \sin (kx + \phi_o)$, positive(negative) ϕ_o means w lags(leads) u. For LSC (as shown in Part 1, Fig. 2), if $u = u_1$ = downwind velocity, $\phi_o = 180°$: if $u = u_2$ = crosswind velocity, $\phi_o = -90°$ at the bottom of the water column and $+90°$ at the top.

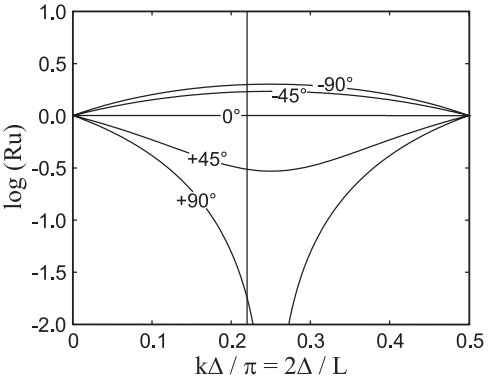

Figure 3. Logarithmic response functions for first-order horizontal velocity variance as a function of $k\Delta/\pi$ and the phase difference ϕ_o between horizontal and vertical components of the turbulent velocity field, for the fixed value of w_o/u =0.577 that gives unit response for $\phi_o = 0°(180°)$. Vertical line as in Figure 2.

80 m scale typical of LSC at LEO15) and fixed w_o/u_o is measured at increasing range, the observed horizontal variance may be either an increasing underestimate, as predicted by Theriault, or an increasing *over*estimate. If the anisotropy ratio itself varies with range, the same fixed wavelength may be underestimated in one part of the range and overestimated in another.

The presence of quasi-deterministic phase relationships between horizontal and vertical velocity components within large-eddy structures adds further complexity. As seen in Figure 3, unit response for fixed $w_o/u_o = 0.577$ and $\phi_o = 0°$ can change dramatically with non-zero ϕ_o. As w progressively lags u (positive ϕ_o), the low-frequency response drops progressively below 1: at $\phi_o = +90°$, the response has a zero at $k\Delta = 0.25$. As w progressively leads u (negative ϕ_o), the low-frequency response rises above 1 to an increasing *maximum* at $k\Delta = 0.25$, before falling to a zero (not shown) at $k\Delta = 0.75$.

Convective records are not characterized by strong phase relationships (see Part 1) and although LSC have quasi-deterministic phase relationships between vertical and horizontal components, the phase between vertical and downwind components is 180°: thus both the convective response and the downwind LSC response should depend primarily on the magnitude of w_o/u_o. In contrast, the phase between vertical and crosswind LSC components varies from $+90°$ at the bottom to $-90°$ at the top of the water column, and for approximately constant w_o/u_o, the phase effect of Figure 3 dominates the crosswind response. The theoretical prediction of quite different LSC responses in downwind and crosswind directions is supported in the following section, where these responses are calculated from LES velocity fields.

The theoretical response function allows comparison of the performance with respect to determination of horizontal velocity variance of different slant beam angles from vertical. Figure 4 compares responses as functions of dimensional wavenumber (necessary because

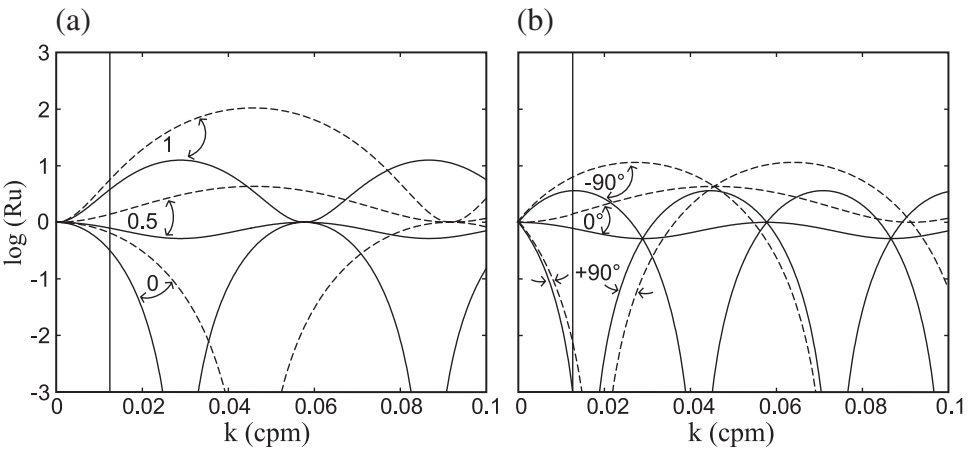

Figure 4. Comparison of logarithmic response functions for first-order horizontal velocity from instruments with slant beam angles from vertical of $\theta = 30°$ (solid lines) and $\theta = 20°$ (dashed lines). The (worst-case) response is calculated at maximum halfwidth $\Delta_M = H \tan\theta$ for the LEO15 value of $H = 15$ m. The vertical line marks the dimensional wavenumber of 0.0125 cpm associated with the ~ 80 m horizontal length scale estimated for observed convective structures and LSC crosswind structure. (a) Variation with w_o/u_o (0, 0.5, 1) for fixed $\phi_o = 0°(180°)$. (b) Variation with ϕ_o ($-90°$, $0°$, $+90°$) for fixed $w_o/u_o = 0.5$.

the parameter Δ used to non-dimensionalize k in Figures 2 and 3 is a function of θ) for the two angles ($\theta = 20°$ and $30°$) available in commercial instruments. With $\phi_o = 0°(180°)$, Figure 4(a) shows that 20° beam angle is preferable for highly anisotropic turbulence (small w_o/u_o), but produces significantly larger overestimation than a 30° instrument when values of w_o/u_o exceed ~ 0.5. For a fixed value of $w_o/u_o = 0.5$ (which lies between the values of 0.377 and 0.577 at which $Ru \equiv 1$ for $\theta = 20°$ and $30°$, respectively), Figure 4(b) illustrates the effects of phase. Response for $\theta = 20°$ is marginally preferable to that for $\theta = 30°$ for $0° < \phi_o < 90°$, but noticeably worse when ϕ_o is negative. These predictions are also confirmed when response functions for both angles are determined from the LES of LSC.

4. Horizontal variance response functions derived from LES of LSC

In the case of Langmuir supercells, response functions for turbulent horizontal variances can be derived from LES available at two values of turbulent Langmuir number $La_t \equiv (u_\tau/u_s)^{1/2}$, where $u_\tau = (\tau_s/\rho_o)^{1/2}$ is the surface friction velocity (τ_s is surface wind stress magnitude and ρ_o water density) and u_s is the surface Stokes drift velocity (McWilliams *et al.,* 1997): for details of the LES, see Tejada-Martínez and Grosch, 2007, henceforth TMG07. Stress forcing was held constant in the simulations, so $La_t = 0.4$ corresponds to stronger Langmuir vortex-forcing than $La_t = 0.7$. Although one might expect stronger vortex forcing to lead to stronger Langmuir cells, the opposite appears to be the case, with

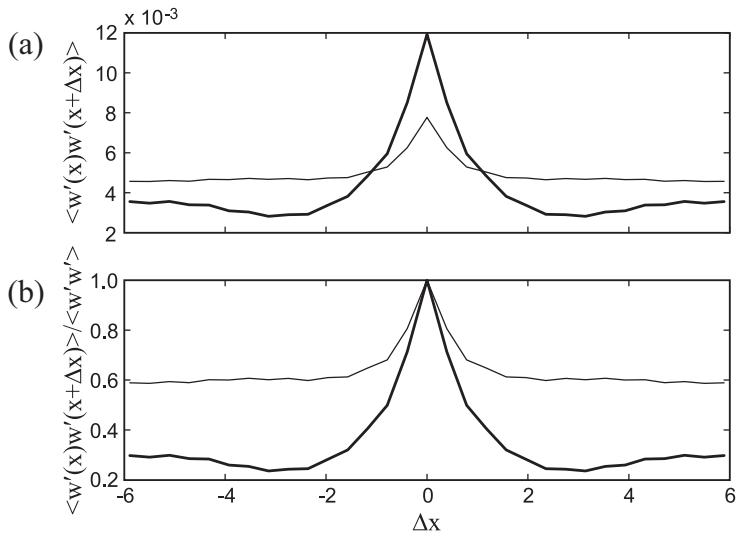

Figure 5. (a) Mid-depth auto-correlation of vertical $w = u_3$ in the downwind direction (here assumed aligned with the instrument x-axis) for flows with $La_t = 0.4$ (heavy curves) and $La_t = 0.7$ (light curves). (b) Same as (a) but normalized by $<u_3'u_3'>$. Although the flow with stronger Langmuir forcing ($La_t = 0.4$) has larger maximum correlation, the normalized correlation drops much more steeply with downwind distance, evidence of shortened downwind length scale.

the $La_t = 0.7$ case exhibiting more distinctly "Langmuir-like" characteristics, specifically more highly linear structures, more intense near bottom downwind "jets", and strong phase relationships among velocity components. With stronger vortex forcing in the $La_t = 0.4$ case, near-bottom downwind "jets" are significantly reduced in magnitude and the elongated downwind structures develop more sinuous structure: Figure 4 illustrates the decreased downwind correlation length scale of the vertical velocity component as La_t decreases from 0.7 to 0.4. Decreased downwind correlation moves the flow toward horizontal isotropy (although the $La_t = 0.4$ flow is by no means yet isotropic) by decreasing the downwind linearity of structures considered characteristic of Langmuir circulations, possibly a progression towards more conventional turbulence through instability of the Langmuir structures.

To derive an LES-based response function, variances of synthetic beam velocities are obtained by sampling the LES fields with the geometry of a VADCP, then averaged over time and both horizontal spatial dimensions of the computational domain used to calculate first-order horizontal variance estimates (for details, see Part 1, Appendix B). Because of the averaging involved, the second-order relationships (e.g., Eq. (11)) are equivalent to the "true" variances, as defined by the LES, and the computational response function is thus the ratio of first-order to second-order computed variances. The response functions Lu_1 and Lu_2 shown in Figure 6, middle panels, are calculated in a horizontal coordinate system oriented in the downwind (subscript 1) and crosswind (subscript 2) directions. Differences

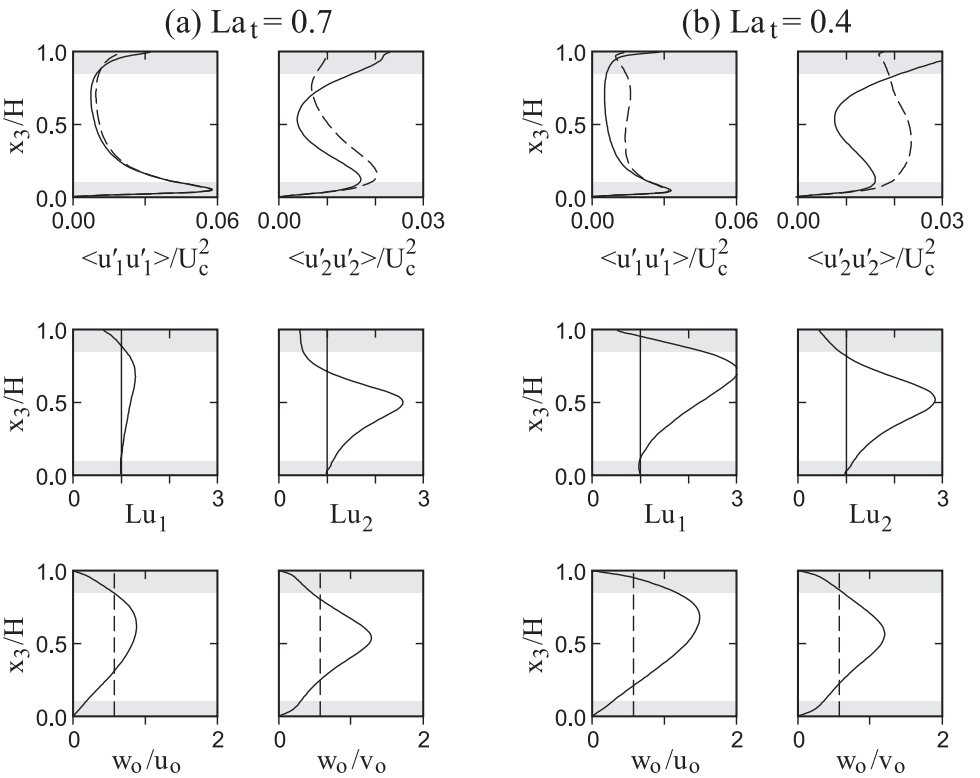

Figure 6. For slant bin angle from vertical θ = 30° and (a) La_t = 0.7 and (b) La_t = 0.4, top panels show profiles of downwind (left) and crosswind (right) horizontal velocity variances normalized with U_c, the mean downwind velocity at mid-depth. Solid lines are the true (LES) values and dashed lines are the first-order estimates. Middle panels are profiles of the LES-derived response functions for the first-order estimates. Bottom panels show the ratios of *rms* vertical to horizontal velocity components $w_o/u_{io} \equiv \langle u_3'u_3' \rangle^{1/2}/\langle u_i'u_i' \rangle^{1/2}$: the vertical dashed line corresponds to the value w_o/u_o = 0.577 theoretically predicted to give unit response for zero phase between vertical and horizontal components. Gray bars indicate areas inaccessible to horizontal velocity observations with the VADCP (θ = 30°) deployed at LEO15.

between Lu_1 and Lu_2 arise from differences in characteristic wavenumber, anisotropy ratio, and phase between horizontal and vertical components associated with the horizontally anisotropic LSC structures. Difference between downwind and crosswind responses is largest in the La_t = 0.7 case, in agreement with previous discussion of the more "Langmuir-like" features of this flow relative to that of La_t = 0.4. As seen in Figure 6, the first-order response is characteristically an over-response in the lower water column, shifting to under-response at a height that varies both with component (the downwind component at a level higher than the crosswind component) and with La_t (the case La_t = 0.4 at a level higher than that of La_t = 0.7). The degree of overestimation of the

downwind component in the middle part of the water column increases with decrease in La_t.

All of the response functions shown in Figure 6 are strikingly different from the increasing-with-height underestimate predicted by the Theriault response function. The theoretical function derived in the previous section aids in understanding that the LES responses result from the presence of vertical velocity fluctuations with magnitude comparable to horizontal fluctuations over much of the interior of the water column (Fig. 6, bottom panels). The observed near-unity downwind response throughout the water column in the $La_t = 0.7$ case (Fig. 6, middle left panel) is predicted by the theory for a structure with (a) the long downwind correlation length scales of the $La_t = 0.7$ case, (b) phase of 180° between u'_1 and $u'_3 = w'$ components, and (c) values of $w_o/u_o \sim 0.6$: slight over-response, as observed in the LES, would be predicted where w_o/u_o approaches 1, around $x_3/H \sim 0.7$. The predicted crosswind response for horizontal wavenumber $k = 2\pi/80$ m typical of LSC is determined mainly by strong phase dependence between u'_2 and u'_3 in LSC (see Part 1, Fig. 2). As illustrated in Figure 3 for $w_o/u_o = 0.577$, unit response near bottom (where Δ is small) is predicted to change to over-response in the lower water column where $\phi_o < 0°$, then to under-response in a near-surface zone where $\phi_o > 0°$. This behavior, which describes the main features of the LES crosswind response for $La_t = 0.7$, would be modulated only slightly by the variation in w_o/u_o with height seen in the lower panels of Figure 6 (left). The more similar (although not identical) downwind and crosswind response functions in the $La_t = 0.4$ case (Fig. 6, middle right panels) would be predicted on the basis of the increase in horizontal isotropy in this case, as suggested by Figure 5.

For anisotropic turbulent structures such as LSC, an additional variable that affects response is the orientation of the ADCP/VADCP instrument to the long axis of the structures. The maximum significant angle ψ between a beam pair axis and the long axis of LSC structures is 45°. For the more anisotropic case of $La_t = 0.7$, Figure 7 compares the response functions for this extreme value of ψ with the case $\psi = 0°$. (Fig. 7(a)) in which the downwind long axis of the cells is assumed to be perfectly aligned with the instrument axis x. As seen previously in Figure 6, response with $\psi = 0°$ is near unity in the x direction (in which $k \rightarrow 0$), but an overestimate in most of the water column for the finite wavenumber of the crosswind structure. As expected, both responses are comparable when the long axis lies mid-way between x and y instrument axes ($\psi = 45°$, Fig. 7(b)), since then both beam pairs sample part of both the larger downwind structure and the smaller crosswind structure. This result suggests that *if* the directionality of turbulent structures is known or suspected *a priori,* installing the ADCP/VADCP at 45° to the dominant direction would produce the most uniform first-order response, an overestimate of both horizontal variances in middle of the water column by a factor of ~ 1.5 for $La_t = 0.7$, ~ 2.7 for $La_t = 0.4$ (not shown).

The LES can be readily re-sampled to investigate the impact of decreased beam angle $\theta = 20°$, allowing an additional comparison with theoretical predictions. As seen in Figure 8,

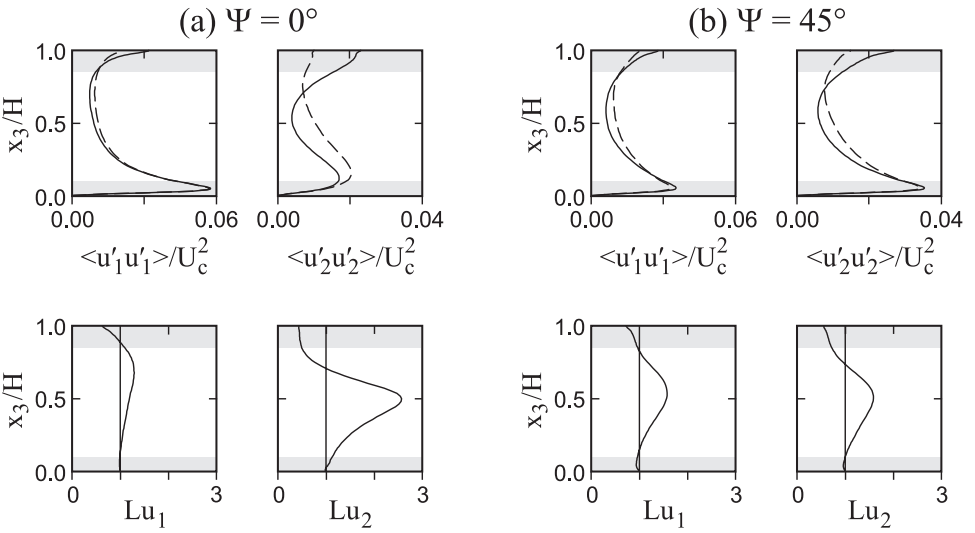

Figure 7. Comparison of response functions for maximum range of angle ψ between one instrument axis and the long axis of strongly directional LSC structures (La_t = 0.7). (a) ψ = 0°, *x* instrument axis aligned with the downwind axis in which LSC are elongated. (b) ψ = 45°. Gray bars indicate areas inaccessible to horizontal velocity observations with the VADCP (θ=30°) deployed at LEO15.

the smaller beam angle approximately doubles over-estimation of horizontal velocity variances in the interior of the water column. This change is qualitatively in agreement with the theoretical curves shown in Figure 4, where for typical interior values of $w_o/u_o >$ 0.5, responses with phases either 0°/180° (Fig. 4(a)) or negative (Fig. 4(b)) are significantly greater for θ = 20° than for θ = 30°, predicting greater over-estimation of downwind variance throughout the water column and of crosswind variance in the lower part of the water column for LSC structures. Thus the cost of the improved slant beam estimation of *vertical* velocity variance with θ = 20° reported in Part 1 is deterioration in estimation of *horizontal* velocity variance. If a fifth vertical beam is available to provide vertical velocity variance directly, a slant beam angle of 30° from vertical, resulting in improved estimation of horizontal variance, is preferable to the now standard 20°.

5. Response functions based on observations of unstable convection and LSC

In Part 1, observational response functions for various slant beam estimates of turbulent vertical velocity variance were determined as ratios of the variance of the slant beam estimate to the "true" variance measured by the vertical beam. The present case of turbulent horizontal velocity variances suffers from lack of independent measures of the true values. With available observational information, only an *estimate* of the response function for the first-order variance can be made. If we assume that the second-order

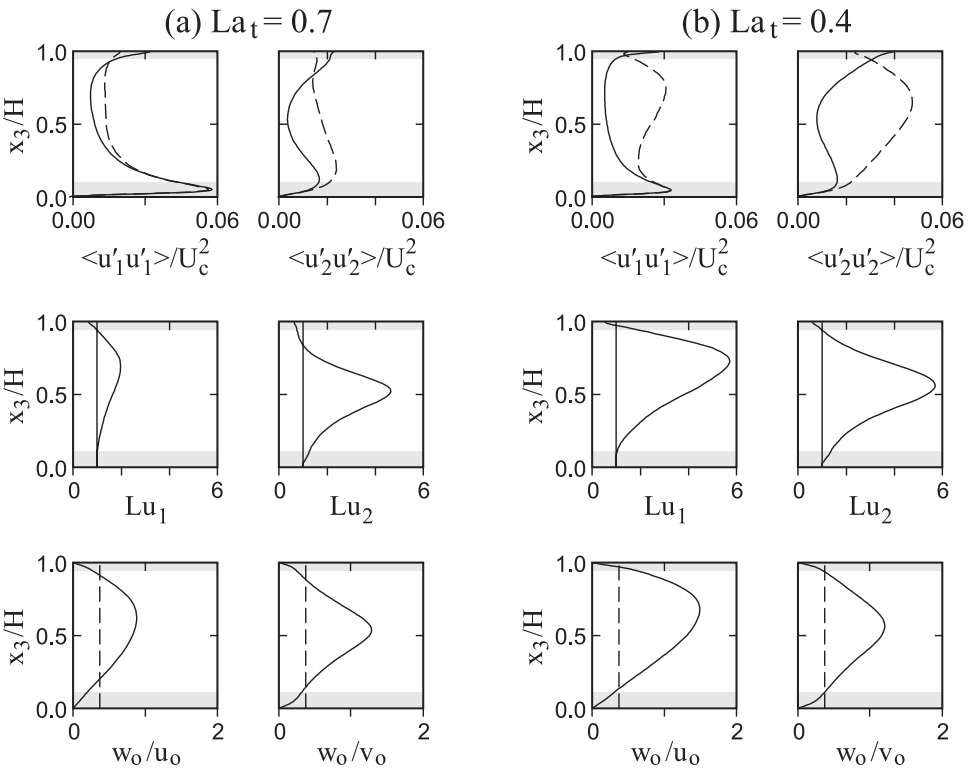

Figure 8. As in Figure 6, except for slant bin angle from vertical $\theta = 20°$ (the vertical dashed line in the bottom panels at $w_o/u_o = 0.377$ is the value theoretically predicted to give unit response with zero phase between vertical and horizontal components for this value of θ). Note the doubling of the horizontal scale of the center panels from Figure 6, necessitated by larger overestimation of horizontal turbulent variances with $\theta = 20°$. Gray bars indicate areas inaccessible to horizontal velocity observations with this ADCP configuration, assuming the same transducer height above bottom as at LEO15.

variance is "true" (or at least closer to "true" than the first-order estimate, since dependent upon less stringent assumptions), estimated response functions (superscript e) can be defined as ratios of first-order to second-order variances, i.e.

$$Ru^e \equiv \langle u'^2 \rangle_{(1)} / \langle u'^2 \rangle_{(2)} \quad \text{and} \quad Rv^e \equiv \langle v'^2 \rangle_{(1)} / \langle v'^2 \rangle_{(2)},$$

where the (u, v) notation draws attention to the fact that primary determination of the ratios occurs in instrument coordinates. Response functions estimated in this way contain unknown uncertainty associated with how close second-order variances really are to "true" variances.

Horizontal velocity variance response functions estimated as described above for the same set of observational records considered in Part 1 exhibit the three archetypal forms

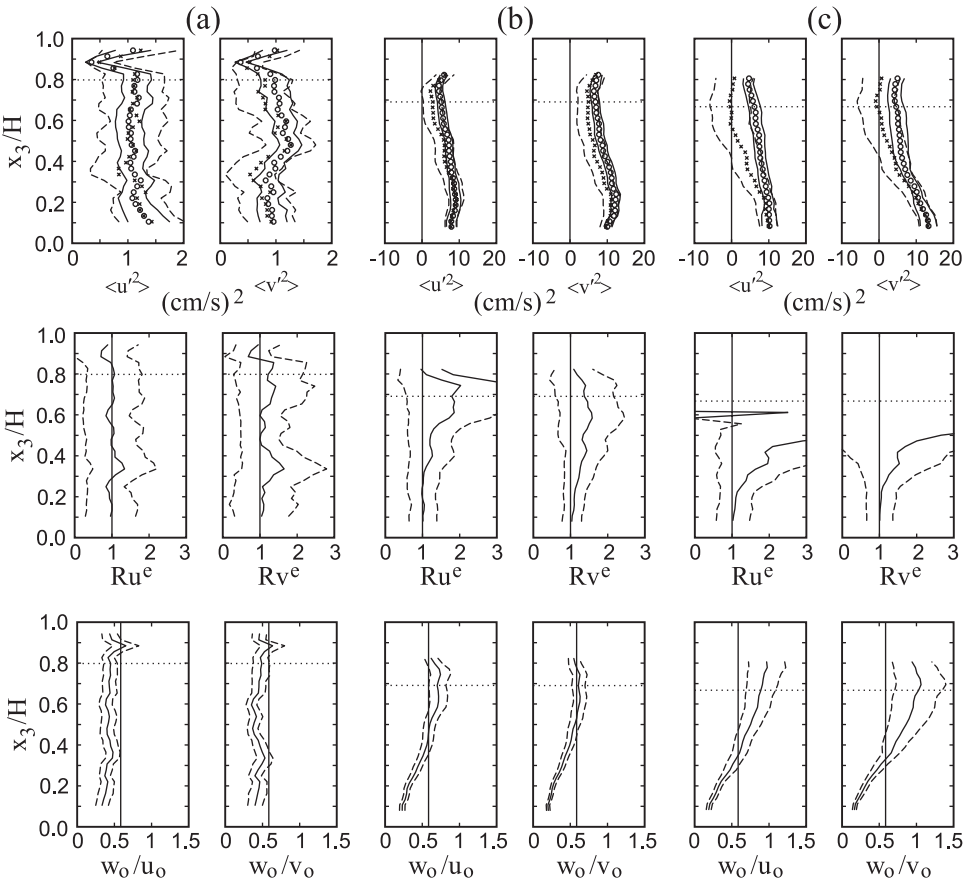

Figure 9. Three archetypes of observationally estimated response functions for horizontal velocity variance. (a) Record 161.006, (b) Record 043.026, (c) Record 043.023. Upper panels: Profiles of horizontal turbulent velocity variances $<u'^2>$ (left) and $<v'^2>$ (right) calculated in instrument coordinates, with one standard deviation error bars (solid and dash lines respectively for first (o) and second (x) order estimates. Middle panels: Response functions (solid lines) for first-order variances, estimated assuming the second-order estimate is accurate, with one standard deviation error bounds (dash lines) calculated as in Appendix A. (c) Profiles of $w_o/u_o \equiv <w'^2>/<u'^2>_{(1)}$ and $w_o/v_o \equiv <w'^2>/<v'^2>_{(1)}$ (solid lines) and one standard deviation error bounds (dash lines). A vertical line in these panels marks the value $w_o/u_o = 0.577$ theoretically predicted to give unit response with zero phase between vertical and horizontal components for $\theta = 30°$. In all panels, the horizontal dashed line marks the nondimensional height above which there is potential for sidelobe contamination of slant beam velocities.

illustrated in Figure 9 (a)–(c). Upper panels are profiles of first and second-order estimates of horizontal variance in instrument coordinates. Variances are corrected for bias errors and (one standard deviation) error bounds are calculated with methods described in Appendix A. The middle panels show the estimated response functions for each compo-

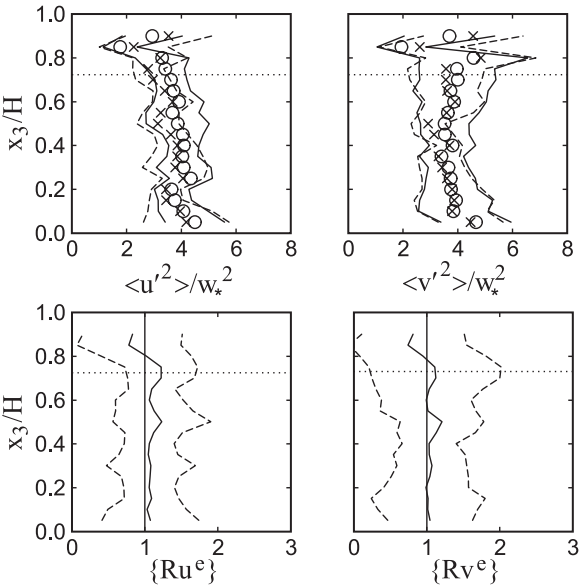

Figure 10. Upper panels: ensemble averages of five convective turbulence records (161.005–161.009). Estimates of horizontal variances, measured in an instrument coordinate system (results are statistically identical in arbitrary horizontal coordinates) are normalized by the convective scale velocity w_* before averaging into bins of scaled height. Lower panels: Ensemble averaged estimated response functions for first-order horizontal variances, with one standard deviation error bounds (dash lines). Symbols as in Figure 9, except that small-sample error bounds are calculated over the ensemble.

nent, while lower panels are profiles of w_o/u_o and w_o/v_o, estimated using vertical beam variance for w_o and first-order horizontal variance for $u_o(v_o)$ (for a reason that will shortly become apparent).

The first archetype, seen in Figure 9(a), is that of convective records. As discussed in Part 1, these are characterized by a distinctive backscatter signature and small O(1 (cm/s)^2) horizontal variances that are quasi-constant with height above bottom and horizontally isotropic, ie independent of horizontal coordinate system. Although the variances are small, both first and second-order estimates are significantly different from zero. Estimated response functions are unity, within rather large error bounds associated with the ratio of two observational values.

In an attempt to reduce the error bounds, ensemble-averaged variance profiles were formed. For each of 5 convective records, dimensional variances were scaled by the convective scale velocity $w_* = 0.55(JH)^{1/3}$ determined with (destabilizing) surface buoyancy flux J and record-average water depth H, then sorted into bins of 0.05 in H-scaled depth. The resulting convective ensemble-average vertical velocity variance is approximately equal to w_*^2 (not shown), while both horizontal variances (Fig. 10) are approximately equal to $4w_*^2$, a value typical of turbulence driven by a mixture of unstable

convection and wind stress in the atmospheric boundary layer (Stull, 1988). These results appear to be the first confirmation of the applicability of this scaling to the ocean. Ensemble-averaged (curly brackets) response functions $\{Ru^e\} \sim \{Rv^e\} \sim 1$, within somewhat reduced error bounds. The observed response is that predicted by the theory of Section 2. In the observed absence of strong phase relationships among velocity components, theoretical response is determined solely by the turbulence isotropy ratio. Estimates of w_o/u_o and w_o/v_o (bottom panels of Fig. 9(a)) are both close to the value of 0.577 theoretically associated with scale-independent unit response, hence consistent with the observationally based near-unity response.

The second archetype, shown in Figure 9(b), is what we will call "normal" LSC records, in which all variance estimates are significantly different from zero: estimated response functions for such records are well-behaved and consistent in character. However because the underlying structures are anisotropic, actual values are expected to depend upon horizontal coordinate system. The instrument coordinate system was by chance approximately 45° to the NE/SW direction of strong wind events at LEO15, hence approximately 45° to the presumed long axis of LSC structures. As expected from the LES results for $\psi = 45°$ discussed above, the two instrument-system response functions (middle panels of Fig. 9(b)) are quite similar, starting at 1 near the transducer and increasing with height to a value of ~ 1.5. However because error bounds for this single record are sufficiently large that a constant response value of 1 cannot be discounted, we again attempt to reduce error bounds by ensemble averaging.

For LSC records, ensemble averaging must be carried out in the "natural" downwind/crosswind coordinate system, lest changes in wind direction between records smear the response. At first-order, horizontal velocity components can be rotated to the desired coordinate system, then squared to form (rotated) variances. However at second-order, the velocity field itself is not calculated, hence the appropriate components of the second-order stress tensor must be rotated (see Appendix B). For consistency of comparison between first and second-order estimates, we first calculate variances of both orders in instrument coordinates, then rotate the stress tensors. (Because the horizontal variance rotation involves $<-u'v'>$, the only shear stress component that does not have a second-order formulation, necessary use of the first-order expression for $<-u'v'>$ (e.g., Eq. (11) of GW07) introduces additional unknown error into rotated results: however as discussed below, this error is likely small for LSC.) After rotation into wind coordinates, variances are normalized by the downwind speed at mid-depth in the water column $U_c \equiv U_1(x_3 = H/2)$ (a parameter readily available from both observations and LES, facilitating comparison between them; see GW07 and TMG07), and sorted before averaging into the same bins of 0.05 in scaled depth used for the convective records.

Differences in scaled variance profiles between the two LSC ensembles seen in Figure 11 probably result mostly from differences in La_t. Observationally determined values (based on a single surface wave at the dominant frequency, see GW07) of $0.52 < La_t < 0.63$ and $0.57 < La_t < 0.72$ for the two sets differ only slightly. However, LES

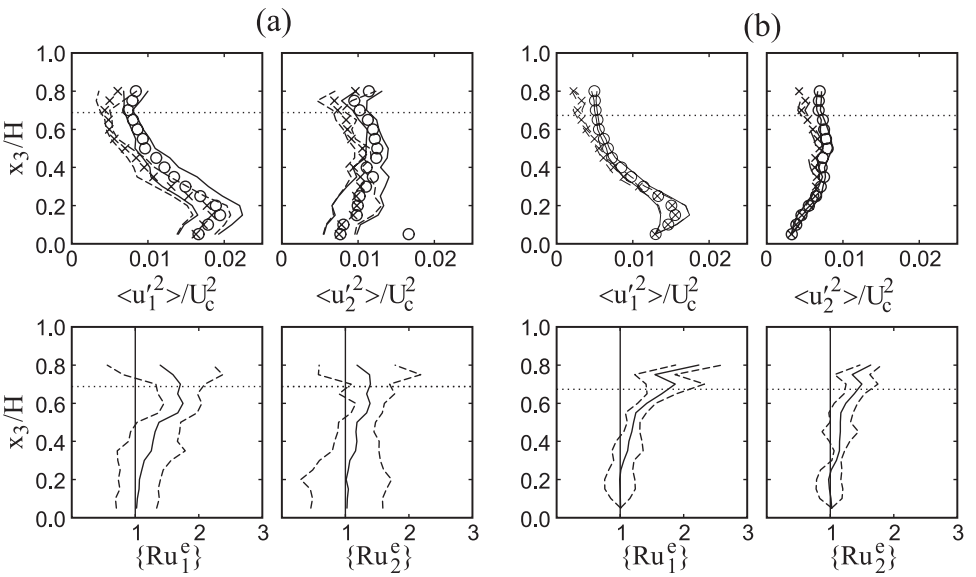

Figure 11. Upper panels: ensemble averages of horizontal velocity variances rotated into downwind (left) and crosswind (right) coordinates, for two sets of "normal" LSC records (a) 043.026, 027 and 028 ($0.52 < La_t < 0.63$) and (b) 154.013, 014 ($0.0.57 < La_t < 0.72$). Variances are scaled by U_c, the downwind speed at mid-depth in the water column, and averaged into scaled depth bins. The two sets are averaged separately because of the observed differences in scaled variance profiles, possibly a result of different La_t. Lower panels: estimated response functions for first-order horizontal variances. Symbols as in Figure 9, except that small-sample error bounds are calculated over the ensemble.

(see TMG07) suggests a high degree of sensitivity to La_t magnitude: thus separate ensemble averages were computed for each episode to avoid having these differences increase error bounds on the computed variance ratio. The basic characteristics of the computed response functions are similar for the two ensembles. Estimated response is close to 1 in the bottom third of the water column, then rises (with now marginal statistical significance) to values of order 1.2 to 1.7 in the remaining part of the water column accessible to the observations. This behavior is in overall agreement with the predictions of both theoretical and LES approaches, although the maximum response magnitude is approximately half that predicted by the LES and subtle differences between downwind and crosswind responses revealed by the LES are obscured by the error in the observational values. Although one of the ensembles (Fig. 11(a)) also shows the tendency towards near-surface underestimation predicted by both theory and LES, these measurements are above the level of potential sidelobe interference in slant beam measurements (horizontal dotted line), hence possibly suspect.

The final archetype is the "abnormal" LSC record of Figure 9(c), in which at least one (and sometimes both) of the second-order variances appears to be significantly underesti-

mated. Underestimation is at its most obvious in a record like that shown, where one of the calculated second-order variances actually becomes negative at heights well below any possibility of sidelobe interference. In less obvious cases, the second-order variances may only become negative after rotation into wind coordinates; in still others, evidence of second-order underestimation lies in sudden increase with height of otherwise normal profiles of the estimated response functions Ru^e and/or Rv^e.

We have considered a number of possible explanations for significant underestimation of second-order variances, focusing on the negative values that are its most obvious manifestation, while noting that negative record-averaged variances are observed only in LSC records and then only in the upper half of the water column.

(1) As shown in Appendix A, second-order variance estimates can be biased either high or low by noise, depending on relative magnitudes of noise level in the vertical and slant beams. For beam noise levels as determined in Part 1, this bias is in the right direction (i.e., the true value is higher than the estimate), but too small in magnitude (i.e., most variances that were negative remain negative when corrected). Thus we dismiss noise bias as an explanation for negative second-order variances.

(2) Negative second-order variances (and the other manifestations of variance underestimation) appear at locations in the water column where both observations and LES indicate minimal horizontal variances, hence might possibly result from inability to resolve small variances. However conversion of profile minimum LES non-dimensional variances of O(0.005) (cf TMG07, Fig. 10(a), $0.5 < x_3/H < 0.7$) to dimensional values using characteristic observed downwind mean speed $U_c \sim 25$ cm/s yields variances of O(3 (cm/s)^2) at this minimum. Since even smaller variances (O(1 (cm/s)^2)) characterize convection, yet negative record-averaged variances are not observed in convective records, we conclude that negative variances in the LSC records are not a result of inability to resolve small variances.

(3) Rotation of horizontal variances to wind-oriented coordinates involves terms $\pm 2 < uv > \sin\alpha \cos\alpha$ (where α is the angle between the wind and one instrument axis, see Appendix B) as well as positive definite terms. Thus depending on the sign of $< uv >$, one or other of the rotated variances could potentially become negative. However because in LSC u' tends to extrema where v' is zero, it seems likely that the correlation between them is small. Even if this were not the case, the $< uv >$ terms cannot account for cases where *both* rotated variances are negative, nor do they serve as an explanation for records (such as that of Fig. 9(c)) in which the variances are negative in the original instrument-based coordinates.

(4) All of the abnormal LSC records are characterized by considerably larger error bounds than the normal records, as illustrated by comparing the archtypes shown in Figure 9(b) and (c). If these larger error bounds were caused by the presence of fewer "structures" within the fixed time extent of one record, the average variance in such records might be closer to the mode than the mean of the probability distribution function for variance. In such records, the estimated value would then be smaller than that for records containing

more structures. However examination of the number of independent estimates in each record revealed no pattern consistent with the hypothesis that negative second-order variances are biased low by small numbers of independently sampled structures: some of the "normal" records had the smallest number of degrees of freedom and a "abnormal" record had the second largest number.

(5) Yet another possibility considered was bias resulting from small non-zero instrument tilt. As detailed in Appendix C, a second-order estimate (subscript 2) made from a tilted {2, 1} beam pair is related to true (unsubscripted) second-order variance by

$$< u'^2 >_{(2)} = < u'^2 > + \phi_3 < u'w' > 2(2 \cot^2 \theta - 1), \tag{14}$$

where $\phi_3 \ll 1$ is the instrument pitch (rotation of the instrument about the axis normal to the plane containing the {2, 1} beam pair, see Appendix C) in radians. A similar relationship involving instrument roll $\phi_2 \ll 1$ can be written for the estimate $<v'v'>_{(2)}$ made from the tilted {4, 3} beam pair. An attractive characteristic of the tilt bias in equation (14) is that it is zero unless turbulent velocity components have coherent phase relationships, ie non-zero $<u'w'>$ covariance, consistent with the absence of negatively biased values in convective cases (which have velocity covariances only $\sim$ one tenth of those associated with LSC records). The θ-dependent multiplier in the bias terms is positive for commercial instruments, so the sign of the tilt bias depends on the signs of the tilt angle and the $<u'w'>$ covariance. We estimate the bias possible in our observational LSC records by using observed tilt values (both pitch and roll are $\sim + 0.2° \sim 0.003$ radians and effectively constant) and LES values of $<u'w'> \sim -2$ (cm/s)^2 at $x_3/H \sim 0.6$. Because $\phi_3 <u'w'> < 0$, the estimated value will be biased low, hence would seem to be a potential explanation for observed negative values. Unfortunately, the magnitude of predicted bias is only ~ 0.07 (cm/s)^2 for $\theta = 30°$, too small to produce negative variance values from true horizontal variance levels of O(3 (cm/s)^2) suggested by the LES. Even allowing for maximum error in the measurement of ϕ_3 (stated error in the tilt sensors is $\pm 0.5°$) raises the potential bias only to ~ -0.2 (cm/s)^2. Moreover since θ, ϕ_2 and ϕ_3 are all fixed, the source of more severe bias in some records relative to others could only lie in different magnitudes of their velocity covariances. Yet the relevant covariances are relatively uniform (within a factor of 2) across the observational LSC records, again arguing that tilt effects were not the prime cause of the observed variance underestimation.

(6) Finally, we examined the possibility that non-Gaussian statistics could lead to bias in the second-order estimate. However using a bootstrap method with replacement (Davidson and Hinkley, 1997) we find that the second-order estimate has effectively zero bias for both normal and abnormal records, removing this as a possible explanation.

In the end, we have not found a convincing explanation for the abnormal archetype. However clear underestimation of horizontal variances by the second-order form in some LSC cases, as evidenced by negative variances calculated in the original instrument coordinate system, advises caution in use of second-order estimates where the underlying

turbulent structures have strong phase correlations among velocity components, this being the only obvious difference between convective and LSC records.

6. Discussion and conclusions

Using a combination of theory, numerical simulation, and observation, we have demonstrated that for structures of horizontal wavelength that is fixed with height above bottom, the first order ADCP estimate of turbulent horizontal velocity variance is not necessarily an underestimate that increases with height, as widely assumed based on the results of Theriault (1986). Instead, all three methods indicate that first-order response can be either an underestimate or an overestimate. We find that, in addition to the angle θ of the slant beams from vertical, the response behavior of first-order estimates depends upon horizontal wavenumber k, the anisotropy ratio w_o/u_o between vertical and horizontal turbulent components, and any quasi-deterministic phase relationships between them, in a manner that is reasonably well described by the theoretical response function derived in Section 3.

For convective turbulence characterized by horizontal isotropy and weak phase relationships among velocity components, the observational response estimated as the ratio of first and second order variances is near unity throughout the water column (Figs. 9(a) and 10). Although we do not have a measurement of the true horizontal variance, this result is internally consistent with theoretical prediction of unit response for a value of $w_o/u_o = 0.577$ and observed quasi-uniform values of ~ 0.5 for that ratio (based on "true" vertical velocity variance from the 5th beam and the first-order estimate for horizontal variance).

In contrast, Langmuir turbulence is characterized by strong phase relationships among velocity components (GW07). Two ensembles of "normal" observationally-based response estimates (Fig. 11) indicate an overestimate that increases with height in most of the water column accessible to the ADCP measurement of horizontal velocities, in qualitative agreement with that derived from the LES of this case. Quantitatively, maximum over-response values of ~ 1.5 for the (wind-coordinate) observational responses are somewhat smaller than LES response maxima, which range up to ~ 3, depending on the value of La_t (Fig. 6).

For the measurement of turbulent horizontal velocity variances, both theoretical and LES results indicate that a system with beam angle $\theta = 30°$ is preferable to the now-standard $\theta = 20°$. For a given turbulent field, the smaller angle is associated with larger variance spread errors (Appendix A), larger bias errors in second-order estimates (Appendix A), and larger tilt biases (Appendix C), while producing greater overestimation of variances for commonly observed values of anisotropy ratio (Figs. 4 and 8).

As was the case with the vertical velocity variance discussed in Part 1, we find encouraging similarity between predicted theoretical responses for first-order horizontal velocity variance and those based on sampling an LES with the geometry of an ADCP. These results suggest that, lacking the gold standard of a response function determined from LES of a particular turbulent flow, the theoretical response function is a useful tool

for estimating response, provided basic characteristics of the large eddies are known at least roughly. The most important characteristics governing response are the characteristic horizontal wavelength of the large eddy structures, their degree of horizontal isotropy, the magnitude of vertical/horizontal anisotropy, and the presence or absence of quasi-deterministic phase relationships among velocity components. All of these characteristics can be estimated from the VADCP data itself. Autocorrelation functions of the individual beam velocities can provide temporal integral scales which can be scaled to horizontal wavelength using measured mean velocity components and Taylor's hypothesis. The degree of horizontal isotropy can be determined by successive horizontal coordinate rotations of these orthogonal length scales, which will be equal and invariant under rotation for horizontally isotropic structures but variable for directional structures. VADCP estimates of vertical to first-order horizontal variances provide at least a gauge of vertical to horizontal isotropy. Very strong phase relationships among velocity components will likely be either obvious, as they are in the case of LSC, or unimportant if not obvious.

While our analyses can be used to assess the degree of error involved in the use of first-order estimates of variance, first-order response would be irrelevant if the second-order estimates suggested by Lohrmann *et al.* (1990) were both available and accurate. Using vertical velocity measured by a vertical beam, we are for the first time able to calculate second-order estimates. Unfortunately, we not only find cases in which horizontal variance is clearly underestimated by the second-order formulation, but have been unable to identify a cause. Until the conditions leading to underestimation of second-order estimates are understood, we suggest that it is safest to use first-order estimates.

For the turbulent flows examined here, the first-order estimates of horizontal velocity variance are accurate to within a factor of 2–3. This level of uncertainty is, as pointed out in the Introduction, approximately the same as that associated with the microscale estimates of large-eddy characteristics that are routinely presented in the literature. As has been the case for dissipation-based estimates, we contend that it is preferable to have somewhat inaccurate estimates of important processes than none at all. At present there are **no** viable alternate techniques that would provide more accurate continuous vertical profiles of three-dimensional turbulent variances over (nearly) the full water column in the shallow coastal oceans that are of such importance to human activities. From autumn through late spring seasons when water column stability is low, convection and Langmuir turbulence appear to dominate vertical and horizontal turbulent transports both at the inner shelf site of the LEO15 data considered here and at the Navy's R2 tower in 26 m depth on the mid-shelf off Georgia (D. Savidge, pers. comm. 2008). Both processes have vertical scale equal to the water column depth and horizontal scales a few to several times larger and neither has been adequately described by standard oceanographic tools. Indeed, the very existence of Langmuir circulations extending to the ocean floor was completely unsuspected until only a few years ago. Until better techniques are devised, ADCPs and VADCPs are the *only* tools available for observational studies of these dominant turbulent processes. Our results will better inform their use.

Acknowledgments. We gratefully acknowledge the support for this research provided by grants from NOAA (NA06RU0139) and NSF (OCE-0136403).

APPENDIX A

Bias and spread of horizontal velocity variance estimates

Estimates of horizontal velocity variance made using squared beam velocities involve errors of both bias and spread (bias error, associated with the presence of (assumed Gaussian random) noise in field measurements, is a positive offset from the "true" value that cannot be reduced by increased sample size, while spread refers to the statistical error associated with finite sample size). The derivations of both types of error follow the techniques described in Part 1, Appendix A, where true beam variance (overbar) is shown to be related to observational variance (angle brackets) by

$$\overline{b_5 b_5} = E(< B_{5f} B_{5f} >) - \sigma_5^2 = < B_{5f} B_{5f} > - \sigma_5^2 \pm s_{55}$$

$$\overline{b_i b_j} = E(< B_{if} B_{jf} >) - \sigma_s^2 = < B_{if} B_{jf} > - \sigma_s^2 \pm s_{ij}, \quad i, j \neq 5.$$

Values of $\sigma_5^2 = 0.10\ (\mathrm{cm/s})^2$ for the noise variance of the vertical beam and $\sigma_s^2 = 0.02\ (\mathrm{cm/s})^2$ for slant beam noise variance (assumed equal for all four beams) are as determined in Part 1: standard deviations over the record length are calculated for individual bins using the method of Heathershaw and Simpson (1978), detailed in Part 1.

It can be shown that the true variance $\overline{u'^2}$ is related to the first-order velocity variance $<u'^2>_{(1)}$ by

$$\begin{aligned}
\overline{u'^2} &= E(<\left(\frac{(B_{2f} - B_{1f}}{2 \sin \theta}\right)^2 >) = (4 \sin^2 \theta)^{-1} E(< B_{2f}^2 + B_{1f}^2 - 2B_{1f}B_{2f} >) \\
&= (4 \sin^2 \theta)^{-1} (E(< B_{1f}^2 >) + E(< B_{2f}^2 >) - 2E(< B_{1f}B_{2f} >)) \\
&= (4 \sin^2 \theta)^{-1} (\overline{b_{1f}^2} + \sigma_s^2 \pm s_{11} + \overline{b_{2f}^2} + \sigma_s^2 \pm s_{22} - 2(\overline{b_{1f}b_{2f}} + \sigma_s^2 \pm s_{12})) \\
&= < u'^2 >_{(1)} \pm \frac{s_{11} + s_{22} + s_{12}}{4 \sin^2 \theta}
\end{aligned}$$

The first-order estimate of horizontal velocity variance is unbiased by noise. The associated spread depends not only upon the measured field, through the standard deviations of beam variances and covariances, but also on slant beam angle from vertical θ. The denominator $4 \sin^2 \theta = 1$ for $\theta = 30°$, but 0.47 for $\theta = 20°$: thus the present commercial standard instrument configuration with $\theta = 20°$ has approximately double the spread error of a 30° instrument.

A similar derivation for the second-order estimate yields

$$\begin{aligned}
\overline{u'^2} &= E\left(\frac{< B_{1f}^2 > - < B_{2f}^2 >}{2 \sin^2 \theta} - < B_{5f}^2 > \cot^2 \theta\right) \\
&= < u'^2 >_{(2)} + \frac{(\sigma_5^2 \cos^2 \theta - \sigma_s^2)}{\sin^2 \theta} \pm \frac{(s_{11} + s_{22} + 2s_{55} \cos^2 \theta)}{2 \sin^2 \theta}
\end{aligned}$$

The second-order estimate of horizontal variance is biased by an amount that depends on both beam noise levels and θ. For fixed values of σ_s^2 and σ_5^2, the difference in $(\sin^2\theta)^{-1}$ (respectively 8.5 and 4 for 20° and 30° instruments) dominates that in $\cos^2\theta$ (respectively 0.93 and 0.75), so the magnitude of the bias (and likely spread) is larger for a 20° instrument. The sign of the bias depends upon the relative magnitudes of σ_s^2 and σ_5^2. With the noise levels of our (30°) instrument, $(\sigma_5^2\cos^2\theta - \sigma_s^2)/\sin^2\theta \sim 0.2$ (cm/s)$^2 > 0$, i.e. the estimate is biased by noise to a value smaller than the true value.

APPENDIX B

Rotation of Reynolds stress tensor into a different horizontal coordinate system

Let $\{u, v, w\}$ be components of horizontal velocity in coordinate system $\{x, y, z\}$ and let the x' axis of coordinate system $\{x', y', z'\}$ be located at angle α, taken as positive for x' to the right of x. In the new coordinate system:

$$u_1' = u\cos\alpha + v\sin\alpha$$

$$u_2' = -u\sin\alpha + v\cos\alpha$$

$$u_3' = w,$$

hence

$$\begin{aligned}
<u_1'^2> &= <(u\cos\alpha + v\sin\alpha)^2> \\
&= <u^2>\cos^2\alpha + <v^2>\sin^2\alpha + 2<uv>\sin\alpha\cos\alpha \\
<u_2'^2> &= <(-u\sin\alpha + v\cos\alpha)^2> \\
&= <u^2>\sin^2\alpha + <v^2>\cos^2\alpha - 2<uv>\sin\alpha\cos\alpha \\
<u_3'^2> &= <w^2> \\
<u_1'u_3'> &= <uw>\cos\alpha + <vw>\sin\alpha \\
<u_2'u_3'> &= -<uw>\sin\alpha + <vw>\cos\alpha \\
<u_1'u_2'> &= <(u\cos\alpha + v\sin\alpha)(-u\sin\alpha + v\cos\alpha)> \\
&= <uv>(\cos^2\alpha - \sin^2\alpha) + (<v^2> - <u^2>)\sin\alpha\cos\alpha
\end{aligned}$$

It is clear from the above that for small values of *both* $<u^2>$ and $<v^2>$, either $<u_1'^2>$ or $<u_2'^2>$ (but not both) can potentially attain negative values, depending upon the sign and magnitude of $<uv>$.

APPENDIX C

Bias of second-order horizontal variance estimates by instrument tilt

Roll (ϕ_2) and pitch (ϕ_3) are defined as the rotation of a vertical plane containing beam pairs {2, 1} and {4, 3} respectively about the axis normal to the plane (see Lu and Lueck, 1999, Fig. 1). For small tilt angles, the beam pair {2, 1} fluctuating beam velocities correct to first-order in ϕ_2 and ϕ_3 (radians) are given by

$$B_{1f} = -u'_+ (\sin\theta + \phi_3 \cos\theta) - w'_+(\cos\theta - \phi_3 \sin\theta) + v'_+\phi_2 \cos\theta \tag{C.1}$$

$$B_{2f} = u'_- (\sin\theta - \phi_3 \cos\theta) - w'_-(\cos\theta + \phi_3 \sin\theta) + v'_-\phi_2 \cos\theta \tag{C.2}$$

where subscripts (+, −) denote values of u', w' measured in beams 1 and 2 at horizontal positions $x_1 = +\Delta(z)$ and $x_2 = -\Delta(z)$ respectively. For the vertical beam,

$$B_{5f} = -(w'_0 - \phi_3 u'_0 - \phi_2 v'_0) \tag{C.3}$$

where the subscript denotes values at $x = 0$.

Using the above relationships with the assumption of second-order homogeneity, i.e. that $<u'^2> = <u'^2_+> = <u'^2_0> = <u'^2_->$, etc.,

$$\frac{<B^2_{1f}> + <B^2_{2f}>}{2\sin^2\theta} = <u'^2> + <w'^2> \cot^2\theta + \phi_3 <u'w'> 2(\cot^2\theta - 1) - \phi_2 <v'w'> 2\cot^2\theta \tag{C.4}$$

and

$$<B^2_{5f}> \cot^2\theta = <w'^2> \cot^2\theta - (\phi_2 <v'w'> + \phi_3 <u'w'>)2\cot^2\theta \tag{C.5}$$

Substituting Eqs. (C.4) and (C.5) in the expression for $<u'^2>_{(2)}$ (text, Eq. 11) yields

$$<u'^2>_{(2)} = <u'^2> + \phi_3 <u'w'> 2(2\cot^2\theta - 1).$$

Similarly, using the {4, 3} beam pair,

$$<v'^2>_{(2)} = <v'^2> + \phi_2 <v'w'> 2(2\cot^2\theta - 1)$$

The θ-dependent multiplier in the bias terms is positive for $\theta < 45°$ (hence for commercially available ADCPs). The tilted estimate of horizontal variance is biased only if there are non-zero phase relationships (i.e., large covariances) between horizontal and vertical turbulent velocity components. The sign of the bias may be either positive or negative, depending on the signs of the relevant tilts and covariances.

REFERENCES

Cheng, R. T., C.-H. Ling, J. W. Gartner and P. F. Wang. 1999. Estimates of bottom roughness length and bottom shear stress in South San Francisco Bay, California. J. Geophys. Res., *104,* 7715–7728.

Davidson, A. C. and D. V. Hinkley. 1997. Bootstrap Methods and Their Application, Cambridge Univ. Press, 582 pp.

Gargett, A. E. 1994. Observing turbulence with a modified acoustic Doppler current profiler. J. Atmos. Oceanic Tech., *11,* 1592–1610.

Gargett, A. E., T. R. Osborn and P. W. Nasmyth. 1984. Local isotropy and the decay of turbulence in a stratified fluid. J. Fluid Mech., *144*, 231–280.

Gargett, A. E., A. E. Tejada-Martínez and C. E. Grosch. 2008. Measuring turbulent large-eddy structures with an ADCP. Part 1. Vertical velocity variance. J. Mar. Res., *66,* 157–189.

Gargett, A. E. and J. R. Wells. 2007. Langmuir turbulence in shallow water. Part.1. Observations. J. Fluid Mech., *576,* 27–61.

Gargett, A. E., J. R. Wells, A. E. Tejada-Martinez and C. E. Grosch. 2004. Langmuir supercells: a mechanism for sediment resuspension and transport in shallow seas. Science, *306,* 1925–1928.

Heathershaw, A. D. and J. H. Simpson. 1978. The sampling variability of the Reynolds stress and its relation to boundary shear stress and drag coefficient measurements. Est. Coastal Mar. Sci., *6,* 263–274.

Lohrmann, A., B. Hackett and L. P. Roed. 1990. High resolution measurements of turbulence, velocity, and stress using a pulse-to-pulse coherent sonar. J. Atmos. Oceanic Tech., *7,* 19–37.

Lu, Y. and R. G. Lueck. 1999. Using a broad-band ADCP in a tidal channel. Part II. Turbulence. J. Atmos. Oceanic Tech., *16,* 1568–1579.

McWilliams, J. C., P. P. Sullivan and C.-H. Moeng. 1997. Langmuir turbulence in the ocean. J. Fluid Mech., *334,* 1–30.

Rippeth, T. P., E. Williams and J. H. Simpson. 2002. Reynolds stress and turbulent energy production in a tidal channel. J. Phys. Oceanogr., *32,* 1242–1251.

Sherwood, C. R., J. R. Lacey and G. Voulgaris. 2006. Shear velocity estimates on the inner shelf off Grays Harbor, Washington, USA. Cont. Shelf Res., *26,* 1995–2018.

Stacey, M. T., S. G. Monismith and J. R. Burau. 1999. Observations of turbulence in a partially stratified estuary. J. Phys. Oceanogr., *29,* 1950–1970.

Stanton, T. P. 2001. A Turbulence-Resolving Coherent Acoustic Sediment Flux Probe Device and Method for Using. US Patent 6,262,942, issued 17 July 2001.

Stull, R. B. 1988. An Introduction to Boundary Layer Meteorology, Kluwer Academic, 666 pp.

Tejada-Martinez, A. E. and C. E. Grosch. 2007. Langmuir turbulence in shallow water: Part II. Large-eddy simulation. J. Fluid Mech., *576,* 63–108.

Theriault, K. B. 1986: Incoherent multibeam Doppler current profiler performance Part II—Spatial response. IEEE J. Oceanic Eng., *OE-11,* 16–25.

Received: *18 November, 2008;* revised: *19 October, 2009.*